

# Large Twist Angle Dependent Ultrafast Transient Dynamics of MoSe<sub>2</sub>/WSe<sub>2</sub> van der Waals Heterostructures beyond the Mott Transition

Vikas Arora<sup>1,2</sup>, Pramoda K Nayak<sup>3,4</sup>, D. V. S. Muthu<sup>1</sup>, A K Sood<sup>\*1,2</sup>

March 3, 2025

<sup>1</sup>*Department of Physics, Indian Institute of Science, Bangalore 560012, India*

<sup>2</sup>*Centre for Ultrafast Laser Applications, Indian Institute of Science, Bangalore 560012, India*

<sup>3</sup>*2D Materials Research and Innovation Group, Department of Physics, Indian Institute of Technology Madras, Chennai 600036, India*

<sup>4</sup>*Centre for Nano and Materials Sciences, Jain (Deemed-to-be University), Jain Global Campus, Kanakpura, Bangalore 562112, Karnataka, India*

**Keywords:** van der Waals Heterostructure, Raman spectroscopy, optical pump-optical probe spectroscopy, ultrafast carrier relaxation dynamics, interlayer excitons, exciton Mott's transition.

## Abstract

Two-dimensional van der Waals heterostructures (HS) exhibit twist-angle ( $\theta$ ) dependent inter-layer charge transfer, driven by moiré potential that tunes the electronic band structure with varying  $\theta$ . Apart from the magic angles of  $\sim 3^\circ$  and  $\sim 57.5^\circ$  that show flat valence bands (twisted WSe<sub>2</sub> bilayer), the commensurate angles of  $21.8^\circ$  and  $38.2^\circ$  reveal the Umklapp light coupling of inter-layer excitons. We report our results on non-degenerate optical pump-optical probe spectroscopy of MoSe<sub>2</sub>/WSe<sub>2</sub> HS at large twist angles under high photoexcitation densities above the Mott transition threshold, generating interlayer localized charge carriers. We show that the recombination time of electrons and holes is minimum at the commensurate angles. The strength of non-radiative interlayer Auger recombination also shows a minimum at the commensurate angles. The fluence

dependence of interlayer carrier recombination time suggests additional relaxation channels near the commensurate angles. This study emphasizes the significance of the large twist angle of HS in developing transition metal dichalcogenides-based optoelectronic devices.

## Introduction

Two-dimensional materials such as graphene, transition metal dichalcogenides (TMDs), and h-BN, along with their heterostructures (HS), show many exciting physical properties. For example, in the case of TMDs, properties such as the large binding energy of excitons [1–3], a strong non-linear optical response [4–6] and spin-valley coupling [7, 8] are exhibited. For the heterobilayers  $\text{MoX}_2/\text{WX}_2$ , the energy levels are decided by  $d$  orbitals of transition metal. The  $5d$  orbital of W is higher than that of the  $4d$  orbital of Mo, and hence, the conduction band minima and valence band maxima of tungsten are higher than that of molybdenum. This creates a staggered or type-II band alignment [9, 10]. This alignment facilitates ultrafast charge transfer between the layers, generation of interlayer exciton with longer decay times [11, 12], and energy transfer among the layers [3, 13]. The optoelectronic properties have been shown to depend on the twist angle between the layers. The twist between the two layers gives rise to a periodic array of potential minima known as the moiré pattern [14–17]. At low temperatures and low twist angles, the multiple sharp peaks superimposed over the photoluminescence (PL) spectra denotes the interlayer excitons trapped in moiré quantum wells [18, 19]. Self-organized quantum dots are observed in  $\text{MoSe}_2/\text{WSe}_2$  and  $\text{MoS}_2/\text{WS}_2$  HS for twist angles less than  $0.5^\circ$  [20]. For  $\text{WS}_2/\text{MoSe}_2$  HS, twist angle tunes the moiré reciprocal lattice and hence the properties of moiré excitons such as oscillator strength and inter/intralayer mixing [21]. In a twisted  $\text{WSe}_2$  bilayer, flat top moiré valence bands are observed at magic angles of  $\sim 3^\circ$  and  $\sim 57.5^\circ$  [22–24]. While small twist angles reveal the properties of moiré excitons, large twist angles describe the characteristics of interlayer excitons.

Nayak *et al.* [10] observed the quenching of photoluminescence for the  $\text{MoSe}_2/\text{WSe}_2$  HS for all the twist angles as compared to constituent monolayers. A redshift in PL energy of up to  $\sim 100$  meV has been observed in HS  $\text{WSe}_2/\text{MoSe}_2$  depending on the twist angle [25, 26]. It has been reported that the PL intensity is two orders lesser for  $\theta = 20^\circ$  as compared to  $\theta = 2^\circ$  for  $\text{MoSe}_2/\text{WSe}_2$  HS [27]. The interlayer distance and binding energy of interlayer exciton are twist-dependent and are maximum at  $30^\circ$ , as revealed by the PL studies [28, 29]. Yu *et al.* have shown that the interlayer excitons undergo Umklapp recombination near the commensurate twist angles of  $21.8^\circ$  and  $38.2^\circ$  [27, 30]. The additional

channel for recombination of interlayer excitons at these particular angles predicts anomalous relaxation dynamics for the HS. The significance of the commensurate angle  $21.8^\circ$  has been emphasized in recent reports on HS MoS<sub>2</sub>/MoSe<sub>2</sub>, demonstrating the highest thermoelectric performance ( $ZT = 2.96$  at  $T = 700$  K) [31] and recording the highest indirect bandgap [32].

A recent report on ultrafast electron diffraction of MoSe<sub>2</sub>/WSe<sub>2</sub> HS indicates that interlayer heat transfer occurs on a  $\sim 20$  ps timescale, mediated by nonthermal phonons followed by interlayer charge transfer and scattering [33]. The ultrafast transient absorption spectroscopy of TMDs HS has shown that the interlayer charge transfer happens on the order of 100 fs time scale [34–39]. A slight variation in geometry or twist angle of the HS can vary the charge transfer time from 100 fs to 1 ps [3, 40, 41]. Zhu *et al.* have reported the recombination time for interlayer exciton in twisted WSe<sub>2</sub>/MoS<sub>2</sub> HS, varying from 40 ps to 3 ns for twist angles between  $0^\circ$  and  $30^\circ$ , and attributed this variation to non-radiative defect-mediated recombination [42]. In this study, no systematic twist-angle dependence of recombination time was observed. We note that these experiments were performed at a fluence of  $\sim 10^{11} \text{cm}^{-2}$ , which is below the exciton Mott transition (MT) [42]. The Mott transition occurs above a certain photoexcitation density, where the distance between excitons becomes smaller than their radius, thus screening the Coulomb interactions between electrons and holes resulting in an unbounded electron-hole plasma [43, 44]. The Mott transition of excitons has been observed in MoSe<sub>2</sub>/WSe<sub>2</sub> HS, where interlayer excitons transform into an electron-hole plasma localized within the individual layers at a photoexcitation density of  $\sim 4 \times 10^{12} \text{cm}^{-2}$ , [45]. An abrupt change in the interlayer exciton photoluminescence linewidth has been observed above the MT photoexcitation density [45, 46]. There have been many reports on different heterostructures for carrier relaxation dynamics but primarily for small twist angles [40, 41, 47], with only a few focusing on large twist angles [42]. All these studies are focused on the photoexcitation densities below the MT. This has motivated us to explore the relaxation dynamics above the exciton Mott transition in TMDs HS with large twist angles.

Here, we report the non-degenerate optical pump-optical probe studies of MoSe<sub>2</sub>/WSe<sub>2</sub> HS at different twist angles at ambient conditions. A significant decrease in the recombination time of interlayer electron-hole plasma near the commensurate angles of  $21.8^\circ$  and  $38.2^\circ$  is observed, which is attributed to additional radiative recombination channels arising from Umklapp recombination. Further, the strength of the interlayer Auger recombination is minimum near the commensurate angles. Our present study can help towards the application of type-II HSs in designing optoelectronic devices, namely photovoltaics, photodetectors, and light-emitting devices where charge transfer and recombination times are important

parameters [48].

## Experimental details

Non-generate optical pump-optical probe measurements were performed using Ti: Sapphire ultrafast laser system (1 kHz repetition rate,  $\sim 50$  fs pulse width, M/s Spectra-Physics, Spitfire Ace) with the pump and probe energies of 3.1 eV and 1.55 eV, respectively. The pump and probe beams are passed collinearly through an objective lens with the NA = 0.9. The spot size of the beam at the sample point was measured to be  $\sim 5$   $\mu\text{m}$ . Experiments were carried out for different twist angles of MoSe<sub>2</sub>/WSe<sub>2</sub> HS at two pump fluences of 2.0 and 2.8 mJ/cm<sup>2</sup> at room temperature.

The MoSe<sub>2</sub>/WSe<sub>2</sub> HS were prepared using the chemical vapor deposition method on a *c*-plane sapphire substrate via a two-step process similar to our earlier work [10]. The individual monolayers of MoSe<sub>2</sub> and WSe<sub>2</sub> have a triangular geometry as shown in the microscopic image of the sample (Figure 1a). The triangles with light (bright) contrast and bigger (smaller) in size represent WSe<sub>2</sub> (MoSe<sub>2</sub>) monolayers as depicted by the black arrows in Figure 1a. A random alignment of triangular-shaped monolayers was obtained as a result of the CVD process, providing us with various twist angles. It has been verified that the TMDs with triangular geometry terminate with transition metal atoms at the edges using transmission electron microscopy [49] and scanning tunneling microscopy [50]. Therefore, the relative orientation of the layers provides us with the angle between the two layers as there is a direct correlation of crystal orientation with the triangular geometry of each monolayer [40, 49, 51]. The twist angle is evaluated as the angle between two lines collinear to the centroid and the vertex of the triangle [52]. One example of evaluating the twist angle is presented in Figure 1b, where red and blue outlined triangles represent MoSe<sub>2</sub> and WSe<sub>2</sub> monolayers, respectively. The lines collinear to the vertex and centroid are the angle bisector in the case of equilateral triangles, which gives the twist angle. The schemes for the front and side view of MoSe<sub>2</sub>/WSe<sub>2</sub> HS for different twist angles are shown elsewhere [10].

## Raman characterization

The blue and red shifts of the A<sub>1g</sub> modes in WS<sub>2</sub> and MoS<sub>2</sub> within their twisted HSs [29] motivated us to perform Raman spectroscopy on HS MoSe<sub>2</sub>/WSe<sub>2</sub> for various twist angles. The group theory for the individual layer provides the irreducible decomposition of Raman active vibration modes A<sub>1g</sub>(R),

$E_{2g}(R)$ , and  $E_{1g}(IR+R)$  for  $MX_2$  monolayer [53]. Figure 2a shows the Raman spectrum of the HS region for a twist angle of  $49^\circ$  recorded using 532 nm laser wavelength. We obtain the following vibration modes as shown in Figure 2a: M1( $MoSe_2$ ,  $A_{1g}$ ):  $238.5\text{ cm}^{-1}$ , M2( $WSe_2$ ,  $A_{1g}+E_{2g}$ ):  $249\text{ cm}^{-1}$ , M3( $WSe_2$ ,  $2LA$ ):  $258.5\text{ cm}^{-1}$ , M4( $MoSe_2$ ,  $E_{2g}$ ):  $286\text{ cm}^{-1}$ , M5( $WSe_2$ ,  $A_2''$ ):  $305\text{ cm}^{-1}$ , M6( $MoSe_2$ ,  $A_2''$ ):  $353\text{ cm}^{-1}$ , M7:  $373\text{ cm}^{-1}$  and M8:  $394\text{ cm}^{-1}$  [54, 55]. It confirms the formation of HS with the presence of all the modes of individual monolayers of  $MoSe_2$  and  $WSe_2$ . From the perspective of the charge transfer among two vertically stacked monolayers, we concentrate on the out-of-plane modes ( $A_{1g}$ ) of the two monolayers  $MoSe_2$  and  $WSe_2$  stacked together, namely M1 ( $MoSe_2$ ) and M2 ( $WSe_2$ ).

Figure S1 (supplementary information) shows the normalized intensities of M1, M2, and M3 with different twist angles. The black dashed lines represent the shift of the peak position of modes M1 or M2 at different twist angles. This systematic behavior of M1 and M2 can be seen in Figure 2b, where the dashed red lines (guides to the eyes) show the opposite slopes for M1 and M2 modes for four different ranges of the twist angles. We observed the softening of M1 and hardening of M2 mode for any non-zero twist angle as compared to the aligned geometry (depicted by blue circles for zero twist angle in Figure S1). Mode M2 starts stiffening as the twist angle is varied till  $17^\circ$ , followed by softening till  $32^\circ$  and then stiffening again till  $39^\circ$  which is again followed by softening. In a counter behavior, the M1 mode softens as the twist angle is varied till  $17^\circ$ , followed by stiffening till  $32^\circ$  and then softening till  $39^\circ$ , which is again followed by stiffening. The softening and stiffening of the  $A_{1g}$  mode (both M1 and M2) depend upon the carrier doping as well as the interlayer coupling [52, 56, 57]. In transition metal dichalcogenide  $MoS_2$ , increasing the number of layers stiffens the  $A_{1g}$  mode and softens the  $E_{2g}$  mode due to increased dielectric screening of Coulomb interactions [58, 59]. It has been reported that the unidirectional transfer of electrons from monolayer  $WS_2$  to monolayer  $MoS_2$  leads to higher carrier density in  $MoS_2$  and lower carrier density in  $WS_2$ , which can soften or stiffen the respective  $A_{1g}$  modes [29]. For the similar staggered bands configuration of HS  $MoSe_2/WSe_2$ , unidirectional electron flow from  $WSe_2$  to  $MoSe_2$  increases (reduces) the carrier density in  $MoSe_2$  ( $WSe_2$ ) and leads to the softening (stiffening) of M1 (M2) modes. To understand the importance of twist angle, we have plotted the difference between the peak position of modes M1 and M2 with twist angles as shown in Figure 2c. A guide to the eye (solid red curve) shows a systematic variation of the shift of M1 with respect to M2 (or vice-versa) with maximum shift near the commensurate angles of  $21.8^\circ$  and  $38.2^\circ$ . For perfectly aligned HS ( $\theta=0^\circ$ ), the electron transfer and the interlayer coupling lead to the softening of  $A_{1g}$  of both M1 and M2 modes, if we compare these modes in monolayers of  $MoSe_2$  and  $WSe_2$  (Figure S1). However, with a non-zero twist angle, variation in the charge transfer and the interlayer coupling tunes the softening

and the corresponding stiffening of M1 and M2 modes and shows an anomalous maximum shift near the commensurate angles. This can be easily understood as the maximum electron transfer and more dielectric screening of Coulomb interaction between electron and hole for the MoSe<sub>2</sub>/WSe<sub>2</sub> HS at these specific angles, which are in the vicinity of commensurate angles. We also note the disappearance of M3 (2LA mode of WSe<sub>2</sub>) at the twist angles of 19° and 39° as depicted by small arrows in Figure S1 (panel iii), which needs further investigation.

## Results and discussions

Figure 3a shows time-resolved differential reflectivity ( $\Delta R/R$ ) for monolayer (ML) MoSe<sub>2</sub> (blue circles), ML WSe<sub>2</sub> (red circles), and HS MoSe<sub>2</sub>/WSe<sub>2</sub> at twist angles ( $\theta$ ) of 20° (pink circles) and 35° (black circles) with a fluence of 2.0 mJ/cm<sup>2</sup>. It demonstrates that the relaxation dynamics for the HS differ from those of the individual MLs and vary with different twist angles. For ML MoSe<sub>2</sub>, a single exponential decay provides a recombination time of 9.6±0.3 ps, whereas ML WSe<sub>2</sub> exhibits a biexponential decay with recombination times of 1.4±0.15 ps and 20.8±0.5 ps. A biexponential fit for the  $\Delta R/R(t)$  (blue circles) for the HS at  $\theta=20^\circ$  is shown by solid red curve in Figure 3b, using the equation:

$$\frac{\Delta R}{R}(t) = \frac{1}{2} \left( 1 + \text{erf} \left( \frac{t - t_0}{\tau_r} \right) \right) (A_1 e^{-t/\tau_1} + A_2 e^{-t/\tau_2} + A_3) \quad (1)$$

where  $(1 + \text{erf}((t - t_0)/\tau_r))$  represents the rise part of the time-resolved  $\Delta R/R$ , with  $\tau_r$  being the rise time, which varies in the range of ~0.7-1.0 ps for different twist angles. The fast and slow recombination processes are characterized by amplitudes and recombination times ( $A_1, \tau_1$ ) and ( $A_2, \tau_2$ ), respectively.  $A_3$  is the strength of the slow relaxation process, taken to be constant in the delay time up to 150 ps. Before extracting the fitting parameters for various twist angles, we discuss the mechanism involved in the relaxation dynamics of HS MoSe<sub>2</sub>/WSe<sub>2</sub>.

Figure 4 shows the type II band alignment in MoSe<sub>2</sub>/WSe<sub>2</sub> HS depicting higher energy states of valence band maxima (VBM) and conduction band minima (CBM) of WSe<sub>2</sub> with respect to that of MoSe<sub>2</sub>. The optical pump excitation using 400 nm (3.1 eV) laser pulse injects carriers into the conduction band much above the band gap for both constituent monolayers (MoSe<sub>2</sub>  $E_g=1.57$  eV, WSe<sub>2</sub>  $E_g=1.67$  eV) [60, 61], as shown in the left panel of Figure 4a. The energetic hot carriers undergo rapid electron-electron scattering and relax to the band edge, followed by a charge transfer between the MLs, creating both inter and intralayer excitons [34, 35]. However, at a photoexcitation density of 2 mJ/cm<sup>2</sup> ( $n_0 \sim 6.1 \times 10^{14}$  cm<sup>-2</sup>), these interlayer excitons undergo Mott transition, where they

transform into a hot electron and hot hole plasma in MoSe<sub>2</sub> and WSe<sub>2</sub> monolayers, respectively [43–46]. These carriers, localized to individual layers, emerge  $\sim 1$  ps after the photoexcitation, when most of the electrons (holes) get transferred to CBM (VBM) of MoSe<sub>2</sub> (WSe<sub>2</sub>) [35, 45], as shown in Figure 4a. Localized interlayer charge carriers take longer to recombine compared to intralayer carriers, as the electrons and holes are confined to different layers rather than being in the same monolayer. The left panel of Figure 4b represents the radiative recombination of the intralayer electrons and holes in the individual monolayers, associated with ( $A_1$ ,  $\tau_1$ ). For WSe<sub>2</sub>/MoSe<sub>2</sub> HS with non-zero twist angle ( $4^\circ \pm 2^\circ$ ), observation of interlayer PL for excitation densities above Mott transition [25, 45] demonstrate the radiative recombination of interlayer electrons and holes, but only at a temperature of 4 K. However, Seyler *et al.* have reported that interlayer electrons and holes in MoSe<sub>2</sub>/WSe<sub>2</sub> do not align at  $\pm K$  valleys in the first Brillouin zone, emphasizing non-radiative recombination as a dominant process [27]. Therefore, we attribute the slow component of the relaxation dynamics ( $A_2$ ,  $\tau_2$ ) to indirect radiative (phonon-mediated) and non-radiative recombination of interlayer electrons and holes, as illustrated in the middle panel of Figure 4b. Motivated by the suggestion of non-radiative Auger recombination of interlayer excitons at high excitation densities [62, 63], the  $A_3$  component is attributed to non-radiative interlayer Auger recombination. In this process, electrons and holes from different MLs recombine and transfer the energy to the third particle, such as an electron or a hole, as demonstrated in the right panel of Figure 4b.

Figure 5a shows the twist-angle ( $\theta$ )-dependent behavior of the intralayer photoexcited carriers ( $A_1$ ) and its recombination time ( $\tau_1$ ) at a fluence of 2.0 mJ/cm<sup>2</sup>.  $A_1$  and  $\tau_1$  exhibit no systematic dependence on twist angle as is expected for intralayer carriers recombination in individual monolayers. The recombination dynamics of the interlayer carriers is presented in Figure 5b, where amplitude  $A_2$  is twist-angle independent. The recombination time of interlayer localized electrons and holes,  $\tau_2$  (panel ii of Figure 5b) exhibits minima near 20° and 38°. The blue dots represent the data, while the solid blue line serves as a guide to the eye. The component associated with non-radiative Auger recombination of interlayer carriers,  $A_3$ , also shows minima for  $\sim 20^\circ$  and  $\sim 38^\circ$  (Figure 5c). The trend of the fitting parameters at a fluence of 2.0 mJ/cm<sup>2</sup> is similar at a fluence of 2.8 mJ/cm<sup>2</sup>, as shown in supplementary Figure S2.

We offer a qualitative understanding of our results. We observed that  $\tau_2$  is maximum at the twist angle of  $\sim 30^\circ$  (Figure 5b), *i.e.* the interlayer localized carriers take the longest time to recombine. This is due to the interlayer distance being maximum at the twist angle of 30° in TMDs HSs [28, 29]. Equally

interesting is the observation of two minima of  $\tau_2$  observed near  $20^\circ$  and  $38^\circ$ . These twist angles are close to the commensurate angles of  $\theta = 21.8^\circ$  and  $38.2^\circ$  for MoSe<sub>2</sub>/WSe<sub>2</sub> HS, where interlayer localized charge carriers or/and excitons can access an additional channel to recombine [27,30]. *Seyler et al.* have demonstrated that for any non-zero twist angle between two layers, the holes in the valence band of WSe<sub>2</sub> and electrons in the conduction band of MoSe<sub>2</sub> at  $\pm K$  points do not align in the first Brillouin zone. However, at the commensurate angle of  $21.8^\circ$ , the valence band and conduction band align at  $\pm K$  points in the second Brillouin zone, as shown in Figure 6, adapted from ref. [27]. At these specific angles, the interlayer charge carriers can recombine radiatively, and the momentum mismatch (due to non-zero twist angle) is compensated by the reciprocal lattice of two layers; the process known as Umklapp recombination [27, 30]. We attribute this Umklapp recombination in the vicinity of commensurate angles as a cause for the two minima observed for  $\tau_2$  (Figure 5b). The two different fluences support the evidence of faster relaxation dynamics in the vicinity of commensurate twist angles. The additional radiative recombination channels for interlayer charge carriers result in lesser interlayer charge carriers involved in non-radiative Auger recombination, leading to a minimum in  $A_3$  near these commensurate angles (Figure 5c). To further investigate the minima for  $\tau_2$  near the commensurate angles, the relaxation dynamics is studied as a function of excitation density for different twist angles.

The fluence dependence of the relaxation dynamics of interlayer charge carriers (Figure 5d) shows an increase in interlayer charge carriers with increasing fluence, which saturates beyond  $2.0 \text{ mJ/cm}^2$  indicating the threshold of charge transfer in HS MoSe<sub>2</sub>/WSe<sub>2</sub> at fluences above  $2.0 \text{ mJ/cm}^2$ . It is important to note that  $\tau_2$  is least fluence dependent at  $20^\circ$  and  $38^\circ$  in comparison to other twist angles, despite a significant increase in the number of interlayer charge carriers. Intralayer charge carriers do not exhibit this distinct behavior near commensurate angles, as shown by the fluence dependence of amplitude  $A_1$  and  $\tau_1$  in supplementary Figure S3. In conclusion, the additional recombination channels for interlayer charge carriers at commensurate angles demonstrate the fluence independence of recombination time ( $\tau_2$ ) within the reported range up to  $2.8 \text{ mJ/cm}^2$ .

## Conclusions

In summary, we have reported the optical pump optical probe spectroscopy of MoSe<sub>2</sub>/WSe<sub>2</sub> HS with different twist angles at high excitation densities above the Mott transition. We observed a significant decrease in interlayer exciton recombination time in the proximity of commensurate angles of  $21.8^\circ$  and

38.2°. We interpret the result as a consequence of the availability of new radiative recombination channels due to Umklapp recombination. The least fluence dependence of interlayer charge carriers recombination time near commensurate angles further supports the presence of additional recombination channels. Our results can be helpful in designing the applications of twisted vdW HS in optoelectronic applications.

## Acknowledgments

AKS thanks the Department of Science and Technology, Government of India, for its financial support under the National Science Chair Professorship and Nanomission (Grant No. DST/NM/TUE/QM-5/2019). DVSM also acknowledges the DST for the Nanomission grant. VA acknowledges CSIR for the research fellowship. PKN acknowledges the MHRD STARS research grant [STARS/APR2019/396] and the support from the Institute of Eminence scheme at IIT-Madras through the 2D Materials Research and Innovation Group.

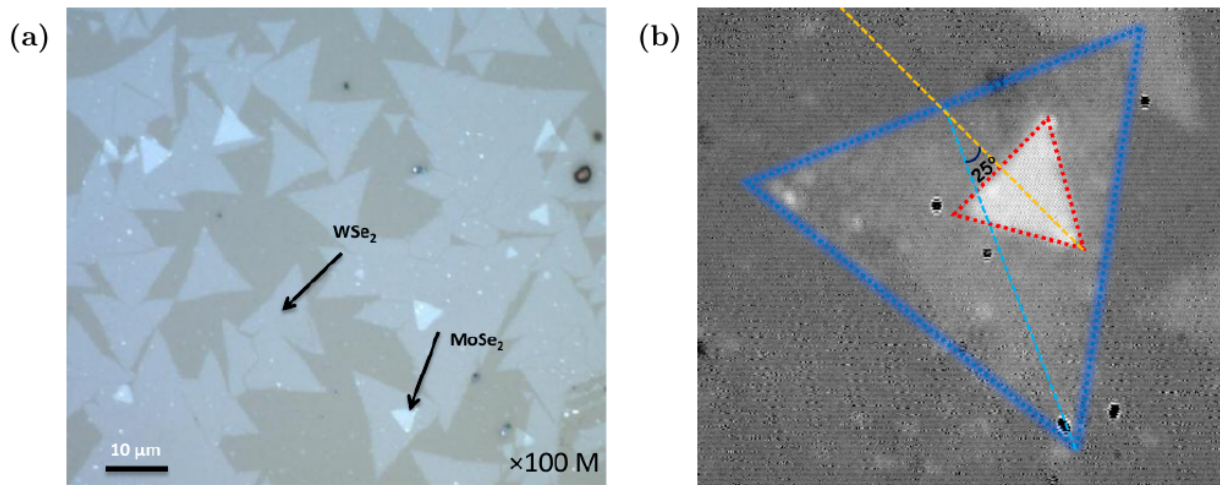


Figure 1: (a) Microscopic image of MoSe<sub>2</sub>/WSe<sub>2</sub> HS depicting WSe<sub>2</sub> as a bottom layer (big triangles) with dull contrast and MoSe<sub>2</sub> as a top layer (smaller triangles) with brighter contrast, (b) Angle evaluation between two monolayers with the blue (red) triangle as a boundary of WSe<sub>2</sub> (MoSe<sub>2</sub>) monolayers.

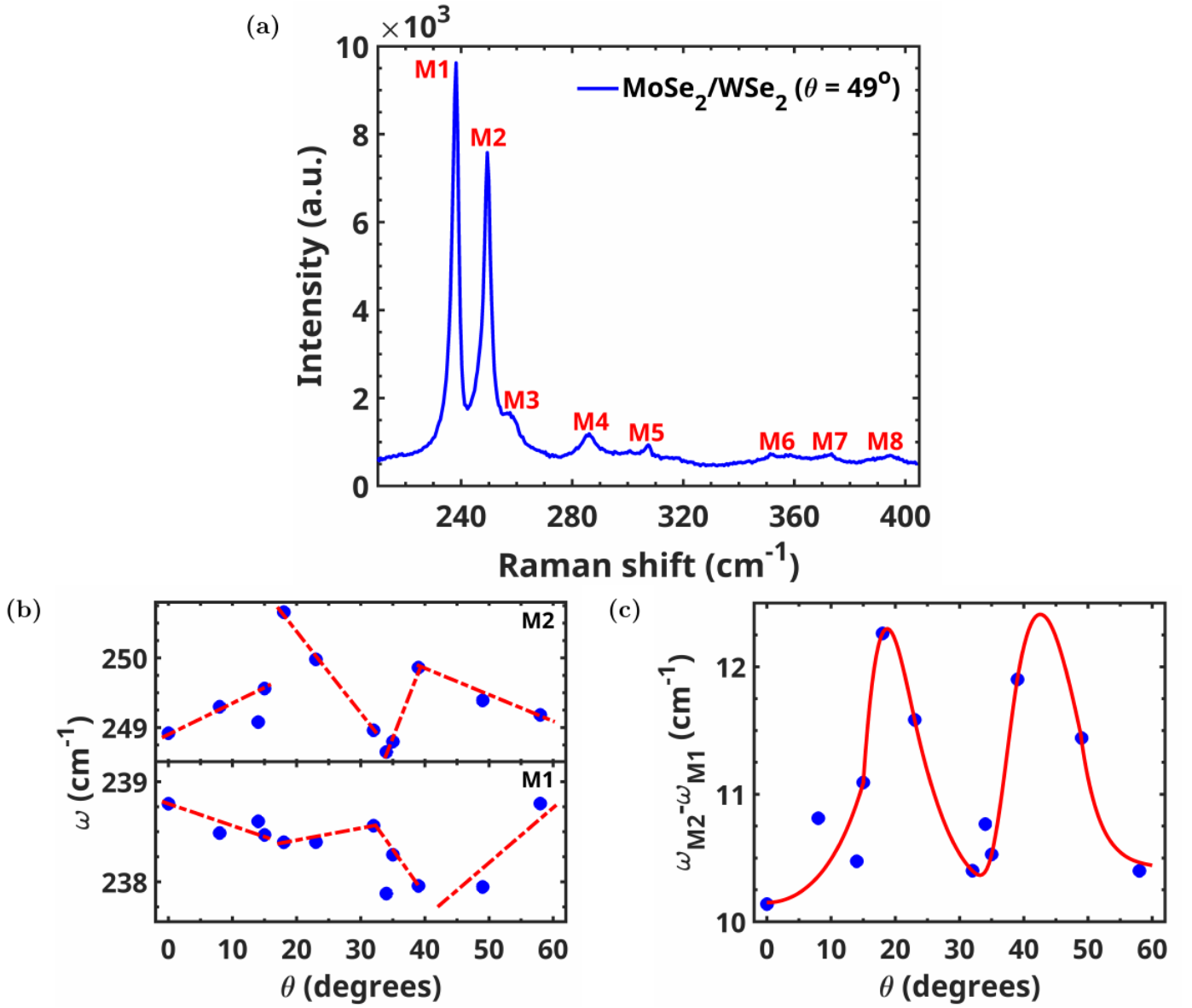


Figure 2: (a) The Raman spectrum for HS at a  $\theta = 49^\circ$ . M1(M2) represents the  $A_{1g}$  mode of  $\text{MoSe}_2(\text{WSe}_2)$ , The respective modes are as follows: M1( $238.5 \text{ cm}^{-1}$ ), M2( $249 \text{ cm}^{-1}$ ), M3( $258.5 \text{ cm}^{-1}$ ), M4( $286 \text{ cm}^{-1}$ ), M5( $305 \text{ cm}^{-1}$ ), M6( $353 \text{ cm}^{-1}$ ), M7( $373 \text{ cm}^{-1}$ ), M8( $394 \text{ cm}^{-1}$ ). (b) The frequency of M1 and M2 modes is plotted as a function of twist angle ( $\theta$ ), the dashed red lines represent the opposite trend of phonon frequencies of M1 and M2 modes with  $\theta$  in the different twist regions, (c) The difference of frequencies of modes M1 and M2 is presented with twist angles. The difference is maximum in the proximity of commensurate angles of  $21.8^\circ$  and  $38.2^\circ$ .

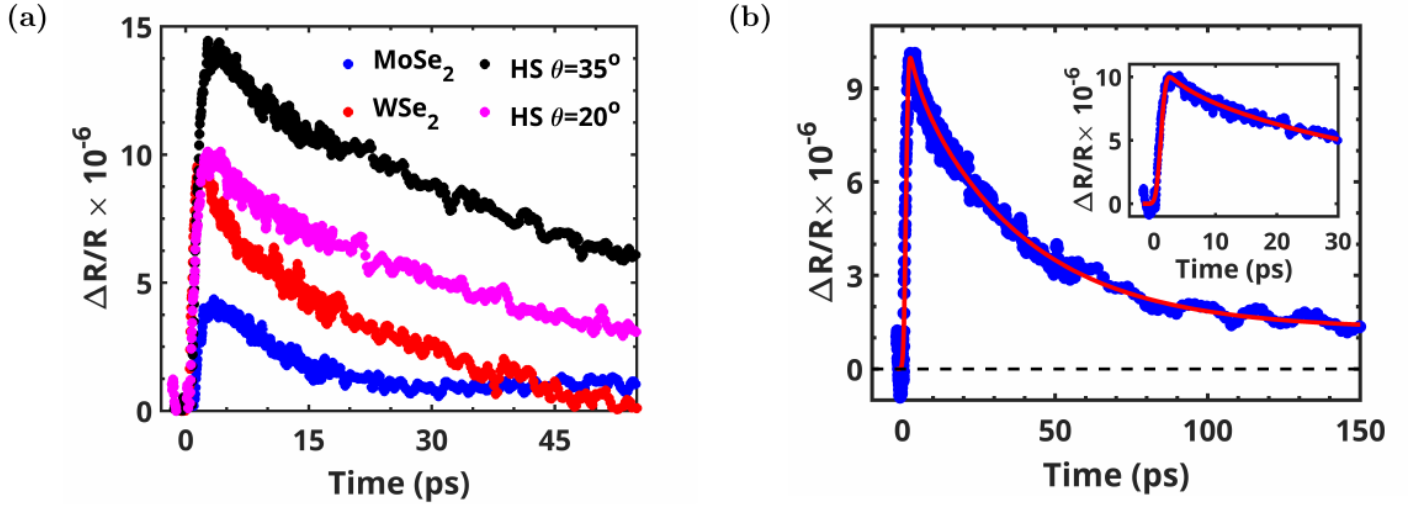


Figure 3: (a) Time evolution of  $\Delta R/R$  for ML MoSe<sub>2</sub> (blue circles), ML WSe<sub>2</sub> (red circles), HS MoSe<sub>2</sub>/WSe<sub>2</sub> at  $\theta=20^\circ$  (pink circles),  $\theta=35^\circ$  (black circles). (b) The differential reflectivity  $\Delta R/R$  for HS MoSe<sub>2</sub>/WSe<sub>2</sub> at twist angle of  $\theta=20^\circ$  (blue circles) is fitted using Eq.(1) (red solid line). The inset shows the fit of the experimental data up to 30 ps.

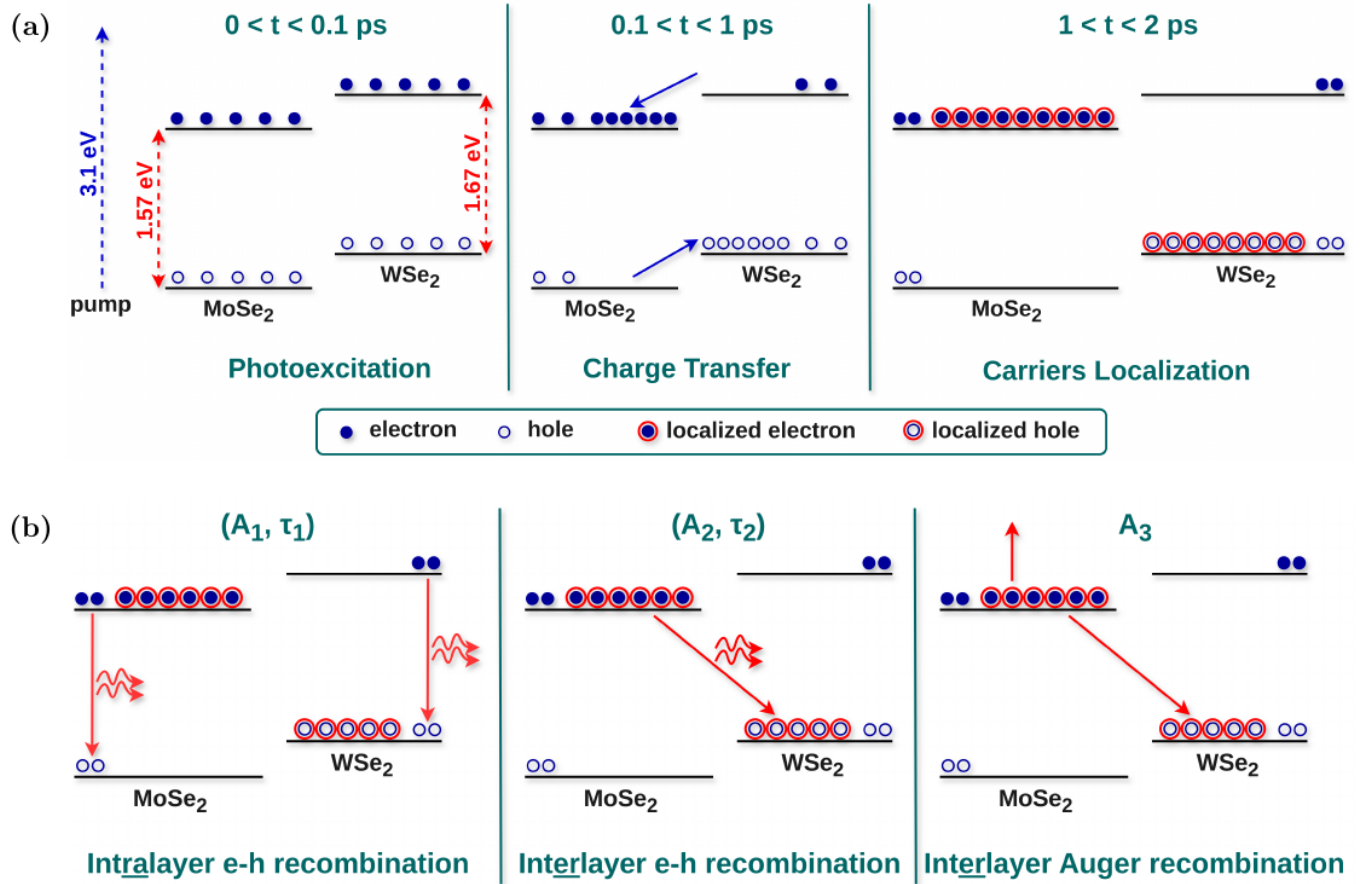


Figure 4: Type II band structure of HS MoSe<sub>2</sub>/WSe<sub>2</sub>, (a) Photoexcitation: Electrons are transferred to the conduction band of MoSe<sub>2</sub> and WSe<sub>2</sub>, Charge transfer: electrons (holes) transfer from conduction (valence) band of WSe<sub>2</sub> (MoSe<sub>2</sub>) to MoSe<sub>2</sub> (WSe<sub>2</sub>), Carriers Localization: interlayer charge carriers localized to distinct individual layers. (b) intralayer e-h recombination (A<sub>1</sub>, τ<sub>1</sub>): electrons and holes within the same layer recombine radiatively, Interlayer e-h recombination (A<sub>2</sub>, τ<sub>2</sub>): Electron and holes in different layers recombine radiatively, Interlayer Auger recombination (A<sub>3</sub>): Electrons and holes in distinct layers recombine non-radiatively, transferring energy to a third particle, which is either an electron or a hole.

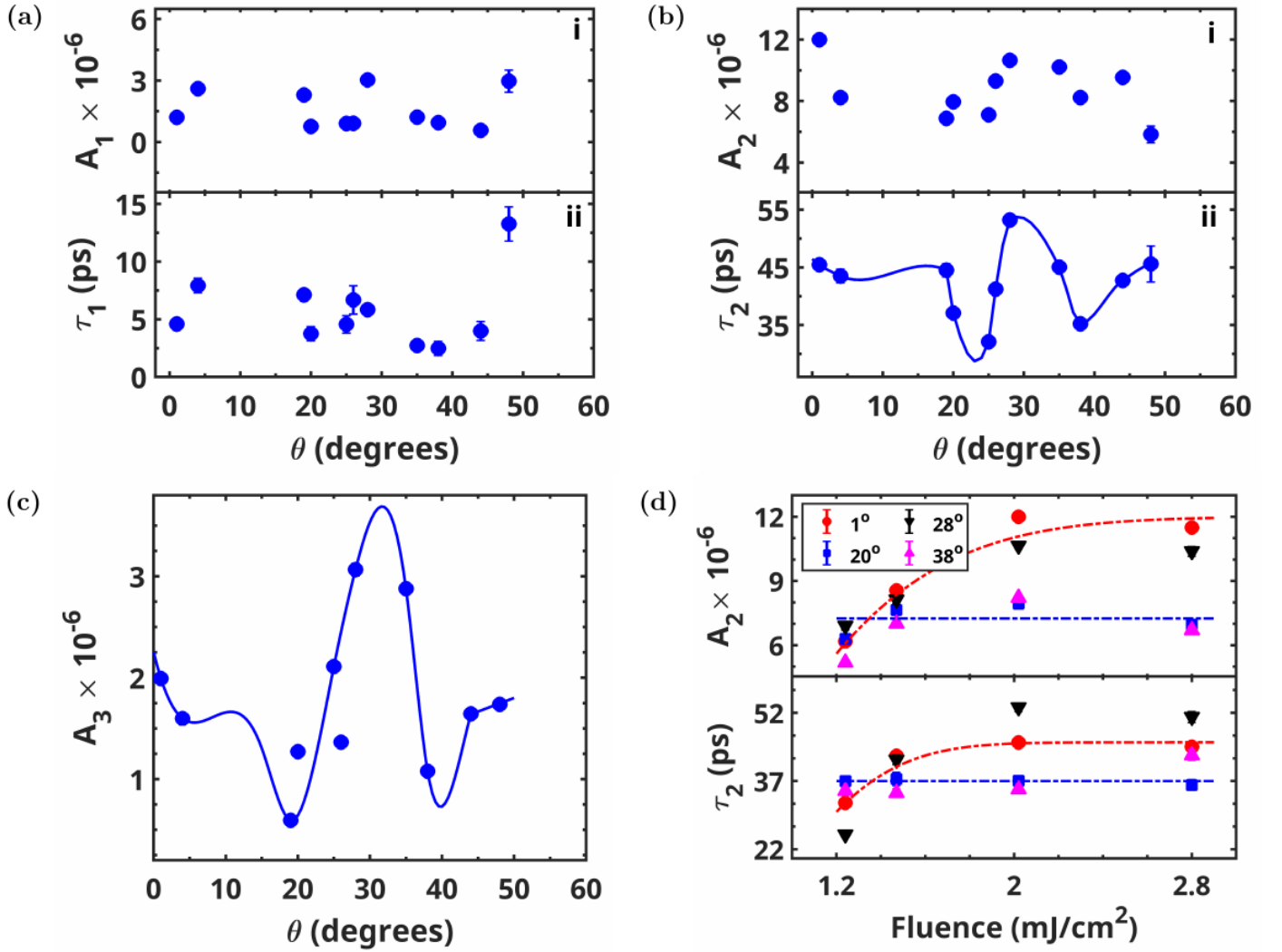


Figure 5: Twist-angle dependence of (a) amplitude ( $A_1$ ) and recombination time ( $\tau_1$ ), (b) amplitude ( $A_2$ ) and recombination time ( $\tau_2$ ), (c) amplitude ( $A_3$ ) at a fluence of  $2.0 \text{ mJ}/\text{cm}^2$ . The solid lines in (b) and (c) are guides to the eyes. (d) Fluence dependence of amplitude ( $A_2$ ) and recombination time ( $\tau_2$ ) for different twist angles. The dashed and dotted (red and blue) lines are guides to the eyes for the data corresponding to  $1^\circ$  and  $20^\circ$

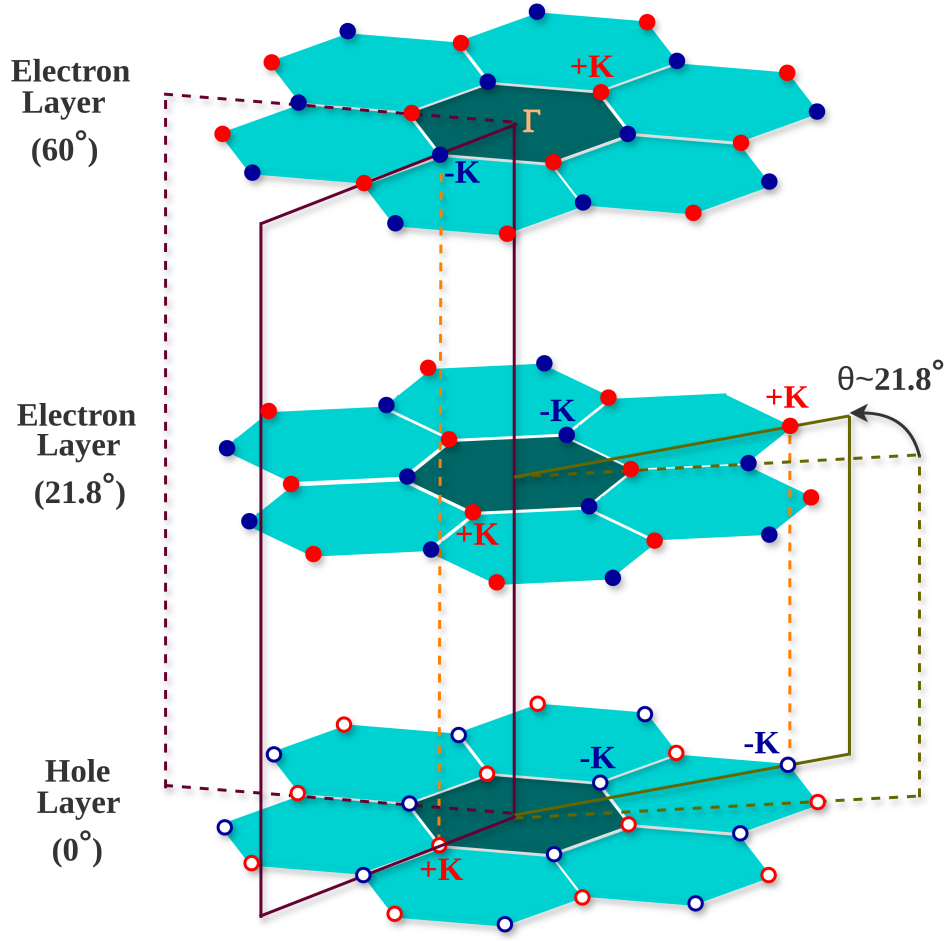


Figure 6: A schematic representation for the valley alignments in the extended Brillouin zone for a twisted HS: The solid and open dots represent the  $-K$ (blue) and  $+K$ (red) valleys in the electron and hole layers. For a twist angle of  $\sim 21.8^\circ$ , the valleys  $+K, -K$  and  $-K, +K$  align in the second Brillouin zone (indicated by an orange dashed line from the middle layer to the bottom layer), which has the same valley pairing for the  $60^\circ$  twisted HS (denoted by the orange dashed line from the top layer to the bottom layers). Consequently, the Umklapp process facilitates the recombination of interlayer excitons at commensurate twist angles. Adapted from *Seyler et al.* [27].

## References

- [1] Alexey Chernikov, Timothy C. Berkelbach, Heather M. Hill, Albert Rigosi, Yilei Li, Burak Aslan, David R. Reichman, Mark S. Hybertsen, and Tony F. Heinz. Exciton binding energy and nonhydrogenic rydberg series in monolayer WS<sub>2</sub>. *Phys. Rev. Lett.*, **113**:076802, (2014).
- [2] Keliang He, Nardeep Kumar, Liang Zhao, Zefang Wang, Kin Fai Mak, Hui Zhao, and Jie Shan. Tightly bound excitons in monolayer WSe<sub>2</sub>. *Phys. Rev. Lett.*, **113**:026803, (2014).
- [3] Yuanyuan Li, Qiannan Cui, Frank Ceballos, Samuel D. Lane, Zeming Qi, and Hui Zhao. Ultrafast interlayer electron transfer in incommensurate transition metal dichalcogenide homobilayers. *Nano Letters*, **17**(11):6661–6666, (2017).
- [4] Nardeep Kumar, Sina Najmaei, Qiannan Cui, Frank Ceballos, Pulickel M. Ajayan, Jun Lou, and Hui Zhao. Second harmonic microscopy of monolayer MoS<sub>2</sub>. *Phys. Rev. B*, **87**:161403, (2013).
- [5] Yilei Li, Yi Rao, Kin Fai Mak, Yumeng You, Shuyuan Wang, Cory R. Dean, and Tony F. Heinz. Probing symmetry properties of few-layer MoS<sub>2</sub> and h-BN by optical second-harmonic generation. *Nano Letters*, **13**(7):3329–3333, (2013).
- [6] Leandro M. Malard, Thonimar V. Alencar, Ana Paula M. Barboza, Kin Fai Mak, and Ana M. de Paula. Observation of intense second harmonic generation from MoS<sub>2</sub> atomic crystals. *Phys. Rev. B*, **87**:201401, (2013).
- [7] Hualing Zeng, Junfeng Dai, Wang Yao, Di Xiao, and Xiaodong Cui. Valley polarization in MoS<sub>2</sub> monolayers by optical pumping. *Nature Nanotechnology*, **7**:490–493, (2012).
- [8] Kin Fai Mak, Keliang He, Jie Shan, and Tony F. Heinz. Control of valley polarization in monolayer MoS<sub>2</sub> by optical helicity. *Nature Nanotechnology*, **7**:494–498, (2012).
- [9] Cheng Gong, Hengji Zhang, Weihua Wang, Luigi Colombo, Robert M. Wallace, and Kyeongjae Cho. Band alignment of two-dimensional transition metal dichalcogenides: Application in tunnel field effect transistors. *Applied Physics Letters*, **103**(5):053513, (2013).
- [10] Pramoda K. Nayak, Yevhen Horbatenko, Seongjoon Ahn, Gwangwoo Kim, Jae-Ung Lee, Kyung Yeol Ma, A-Rang Jang, Hyunseob Lim, Dogyeong Kim, Sunmin Ryu, Hyeonsik Cheong, Noejung Park, and Hyeon Suk Shin. Probing evolution of twist-angle-dependent interlayer excitons in MoSe<sub>2</sub>/WSe<sub>2</sub> van der waals heterostructures. *ACS Nano*, **11**(4):4041–4050, (2017).

- [11] Torben L. Purz, Eric W. Martin, Pasqual Rivera, William G. Holtzmann, Xiaodong Xu, and Steven T. Cundiff. Coherent exciton-exciton interactions and exciton dynamics in a MoSe<sub>2</sub>/WSe<sub>2</sub> heterostructure. *Phys. Rev. B*, **104**:L241302, (2021).
- [12] John R. Schaibley. Control of interlayer valley excitons in atomically-thin MoSe<sub>2</sub>-WSe<sub>2</sub> heterostructures. In *OPTO*, (2017).
- [13] Yan Zeng, Wei Dai, Rundong Ma, Zhe Li, Zhenwei Ou, Cheng Wang, Yiling Yu, Tong Zhu, Xiaoze Liu, Ti Wang, and Hongxing Xu. Distinguishing ultrafast energy transfer in atomically thin MoS<sub>2</sub>/WS<sub>2</sub> heterostructures. *Small*, **18**(44):2204317, (2022).
- [14] Kha Tran, Galan Moody, Fengcheng Wu, Xiaobo Lu, Junho Choi, Kyoungwan Kim, Amritesh Rai, Daniel A. Sanchez, Jiamin Quan, Akshay Singh, Jacob Embley, André Zepeda, Marshall Campbell, Travis Autry, Takashi Taniguchi, Kenji Watanabe, Nanshu Lu, Sanjay K. Banerjee, Kevin L. Silverman, Suenne Kim, Emanuel Tutuc, Li Yang, Allan H. MacDonald, and Xiaoqin Li. Evidence for moiré excitons in van der waals heterostructures. *Nature*, **567**(7746):71–75, (2019).
- [15] Chenhao Jin, Emma C. Regan, Aiming Yan, M. Iqbal Bakti Utama, Danqing Wang, Sihan Zhao, Ying Qin, Sijie Yang, Zhiren Zheng, Shenyang Shi, Kenji Watanabe, Takashi Taniguchi, Sefaattin Tongay, Alex Zettl, and Feng Wang. Observation of moiré excitons in WSe<sub>2</sub>/WS<sub>2</sub> heterostructure superlattices. *Nature*, **567**(7746):76–80, (2019).
- [16] James G. McHugh, Vladimir V. Enaldiev, and Vladimir I. Fal’ko. Moiré superstructures in marginally twisted NbSe<sub>2</sub> bilayers. *Phys. Rev. B*, **108**:224111, Dec (2023).
- [17] Niclas Götting, Frederik Lohof, and Christopher Gies. Moiré-bose-hubbard model for interlayer excitons in twisted transition metal dichalcogenide heterostructures. *Phys. Rev. B*, **105**:165419, (2022).
- [18] Zidong Li, Xiaobo Lu, Darwin F. Cordovilla Leon, Zhengyang Lyu, Hongchao Xie, Jize Hou, Yanzhao Lu, Xiaoyu Guo, Austin Kaczmarek, Takashi Taniguchi, Kenji Watanabe, Liuyan Zhao, Li Yang, and Parag B. Deotare. Interlayer exciton transport in MoSe<sub>2</sub>/WSe<sub>2</sub> heterostructures. *ACS Nano*, **15**(1):1539–1547, (2021).
- [19] Michael Förg, Anvar S. Baimuratov, Stanislav Yu. Kruchinin, Ilia A. Vovk, Johannes Scherzer, Jonathan Förste, Victor Funk, Kenji Watanabe, Takashi Taniguchi, and Alexander Högele. Moiré

- excitons in MoSe<sub>2</sub>-WSe<sub>2</sub> heterobilayers and heterotrilayers. *Nature Communications*, **12**:1656, (2021).
- [20] V. V. Enaldiev, F. Ferreira, J. G. McHugh, and Vladimir I. Fal'ko. Self-organized quantum dots in marginally twisted MoSe<sub>2</sub>/WSe<sub>2</sub> and MoS<sub>2</sub>/WS<sub>2</sub> bilayers. *npj 2D Materials and Applications*, **6**(1):74, (2022).
- [21] Long Zhang, Zhe Zhang, Fengcheng Wu, Danqing Wang, Rahul Gogna, Shaocong Hou, Kenji Watanabe, Takashi Taniguchi, Krishnamurthy Kulkarni, Thomas Kuo, Stephen R. Forrest, and Hui Deng. Twist-angle dependence of moiré excitons in WS<sub>2</sub>/MoSe<sub>2</sub> heterobilayers. *Nature Communications*, **11**(1):5888, (2020).
- [22] Zhiming Zhang, Yimeng Wang, Kenji Watanabe, Takashi Taniguchi, Keiji Ueno, Emanuel Tutuc, and Brian J. LeRoy. Flat bands in twisted bilayer transition metal dichalcogenides. *Nature Physics*, **16**(11):1093–1096, (2020).
- [23] Trithep Devakul, Valentin Crépel, Yang Zhang, and Liang Fu. Magic in twisted transition metal dichalcogenide bilayers. *Nature Communications*, **12**(1):6730, (2021).
- [24] Mit H. Naik and Manish Jain. Ultraflatbands and shear solitons in Moiré patterns of twisted bilayer transition metal dichalcogenides. *Phys. Rev. Lett.*, **121**:266401, (2018).
- [25] Chirag Chandrakant Palekar, Joakim Hagel, Barbara Rosa, Samuel Brem, Ching-Wen Shih, Imad Limame, Martin von Helversen, Sefaattin Tongay, Ermin Malic, and Stephan Reitzenstein. Anomalous redshift in interlayer exciton emission with increasing twist angle in WSe<sub>2</sub>/MoSe<sub>2</sub> heterostructures. *2D Materials*, **11**(2):025034, (2024).
- [26] Kai Wang, Bing Huang, Mengkun Tian, Frank Ceballos, Ming-Wei Lin, Masoud Mahjouri-Samani, Abdelaziz Boulesbaa, Alexander A. Puretzy, Christopher M. Rouleau, Mina Yoon, Hui Zhao, Kai Xiao, Gerd Duscher, and David B. Geohegan. Interlayer coupling in twisted WSe<sub>2</sub>/WS<sub>2</sub> bilayer heterostructures revealed by optical spectroscopy. *ACS Nano*, **10**(7):6612–6622, (2016).
- [27] Kyle L. Seyler, Pasqual Rivera, Hongyi Yu, Nathan P. Wilson, Essance L. Ray, David G. Mandrus, Jiaqiang Yan, Wang Yao, and Xiaodong Xu. Signatures of moiré-trapped valley excitons in MoSe<sub>2</sub>/WSe<sub>2</sub> heterobilayers. *Nature*, **567**:66–70, (2019).

- [28] Ke Wu, Hongxia Zhong, Quanbing Guo, Jibo Tang, Jing Zhang, Lihua Qian, Zhifeng Shi, Chendong Zhang, Shengjun Yuan, Shunping Zhang, and Hongxing Xu. Identification of twist-angle-dependent excitons in  $\text{WS}_2/\text{WSe}_2$ . *National Science Review*, **9**, (2021).
- [29] Lishu Wu, Chunxiao Cong, Jingzhi Shang, Weihuang Yang, Yu Chen, Jiadong Zhou, Wei Ai, Yanlong Wang, Shun Feng, Hongbo Zhang, Zheng Liu, and Ting Yu. Raman scattering investigation of twisted  $\text{WS}_2/\text{MoS}_2$  heterostructures: interlayer mechanical coupling versus charge transfer. *Nano Research*, **14**:2215–2223, (2021).
- [30] Hongyi Yu, Yong Wang, Qingjun Tong, Xiaodong Xu, and Wang Yao. Anomalous light cones and valley optical selection rules of interlayer excitons in twisted heterobilayers. *Phys. Rev. Lett.*, **115**:187002, (2015).
- [31] Hanping Xiong, Xianhua Nie, Li Zhao, and Shuai Deng. Engineering symmetry breaking in twisted  $\text{MoS}_2/\text{MoSe}_2$  heterostructures for optimal thermoelectric performance. *ACS Applied Materials & Interfaces*, **16**(19):25124–25135, (2024). PMID: 38709893.
- [32] Saurav Sachin, Puja Kumari, Neelam Gupta, Shivani Rani, Subhasmita Kar, and Soumya Jyoti Ray. Van der waals twistronics in a  $\text{MoS}_2/\text{WS}_2$  heterostructure. *Computational Condensed Matter*, **35**:e00797, (2023).
- [33] Amalya C. Johnson, Johnathan D. Georganas, Xiaozhe Shen, Helen Yao, Ashley P. Saunders, Helen J. Zeng, Hyungjin Kim, Aditya Sood, Tony F. Heinz, Aaron M. Lindenberg, Duan Luo, Felipe H. da Jornada, and Fang Liu. Hidden phonon highways promote photoinduced interlayer energy transfer in twisted transition metal dichalcogenide heterostructures. *Science Advances*, **10**(4):eadj8819, (2024).
- [34] Xiaoping Hong, Jonghwan Kim, Su-Fei Shi, Yu Zhang, Chenhao Jin, Yinghui Sun, Sefaattin Tongay, Junqiao Wu, Yanfeng Zhang, and Feng Wang. Ultrafast charge transfer in atomically thin  $\text{MoS}_2/\text{WS}_2$  heterostructures. *Nature Nanotechnology*, **9**(9):682–686, (2014).
- [35] Frank Ceballos, Matthew Z. Bellus, Hsin-Ying Chiu, and Hui Zhao. Ultrafast charge separation and indirect exciton formation in a  $\text{MoS}_2$ - $\text{MoSe}_2$  van der waals heterostructure. *ACS Nano*, **8**(12):12717–12724, (2014).
- [36] Frank Ceballos, Matthew Z. Bellus, Hsin-Ying Chiu, and Hui Zhao. Probing charge transfer excitons in a  $\text{MoSe}_2$ - $\text{WS}_2$  van der waals heterostructure. *Nanoscale*, **7**:17523–17528, (2015).

- [37] Bo Peng, Yu Guannan, Liu Xinfeng, Bo Liu, Xiao Liang, Lei Bi, Longjiang Deng, Tze Chien Sum, and Kian Ping Loh. Ultrafast charge transfer in MoS<sub>2</sub>/WSe<sub>2</sub> p–n heterojunction. *2D Materials*, **3**(2):025020, (2016).
- [38] Peymon Zereshki, Yaqing Wei, Run Long, and Hui Zhao. Layer-coupled states facilitate ultrafast charge transfer in a transition metal dichalcogenide trilayer heterostructure. *The Journal of Physical Chemistry Letters*, **9**(20):5970–5978, (2018).
- [39] R. Krause, S. Aeschlimann, M. Chávez-Cervantes, R. Perea-Causin, S. Brem, E. Malic, S. Forti, F. Fabbri, C. Coletti, and I. Gierz. Microscopic understanding of ultrafast charge transfer in van der waals heterostructures. *Phys. Rev. Lett.*, **127**:276401, (2021).
- [40] Ziheng Ji, Hao Hong, Jin Zhang, Qi Zhang, Wei Huang, Ting Cao, Ruixi Qiao, Can Liu, Jing Liang, Chuanhong Jin, Liying Jiao, Kebin Shi, Sheng Meng, and Kaihui Liu. Robust stacking-independent ultrafast charge transfer in MoS<sub>2</sub>/WS<sub>2</sub> bilayers. *ACS Nano*, **11**(12):12020–12026, (2017).
- [41] Jin Zhang, Hao Hong, Chao Lian, Wei Ma, Xiaozhi Xu, Xu Zhou, Huixia Fu, Kaihui Liu, and Sheng Meng. Interlayer-state-coupling dependent ultrafast charge transfer in MoS<sub>2</sub>/WS<sub>2</sub> bilayers. *Advanced Science*, **4**(9):1700086, (2017).
- [42] Haiming Zhu, Jue Wang, Zizhou Gong, Young Duck Kim, James Hone, and X.-Y. Zhu. Interfacial charge transfer circumventing momentum mismatch at two-dimensional van der Waals heterojunctions. *Nano Letters*, **17**(6):3591–3598, (2017).
- [43] E. Hendry, M. Koeberg, and M. Bonn. Exciton and electron-hole plasma formation dynamics in ZnO. *Phys. Rev. B*, **76**:045214, (2007).
- [44] Gabija Kiršanskė, Petru Tighineanu, Raphaël S. Daveau, Javier Miguel-Sánchez, Peter Lodahl, and Søren Stobbe. Observation of the exciton Mott transition in the photoluminescence of coupled quantum wells. *Phys. Rev. B*, **94**:155438, (2016).
- [45] Jue Wang, Jenny Ardelean, Yusong Bai, Alexander Steinhoff, Matthias Florian, Frank Jahnke, Xiaodong Xu, Mackillo Kira, James Hone, and X.-Y. Zhu. Optical generation of high carrier densities in 2D semiconductor heterobilayers. *Science Advances*, **5**(9):eaax0145, (2019).
- [46] M. Stern, V. Garmider, V. Umansky, and I. Bar-Joseph. Mott transition of excitons in coupled quantum wells. *Phys. Rev. Lett.*, **100**:256402, (2008).

- [47] Albert F. Rigosi, Heather M. Hill, Yilei Li, Alexey Chernikov, and Tony F. Heinz. Probing interlayer interactions in transition metal dichalcogenide heterostructures by optical spectroscopy: MoS<sub>2</sub>/WS<sub>2</sub> and MoSe<sub>2</sub>/WSe<sub>2</sub>. *Nano Letters*, **15**(8):5033–5038, (2015).
- [48] Yuan Liu, Nathan O. Weiss, Xidong Duan, Hung-Chieh Cheng, Yu Huang, and Xiangfeng Duan. Van der waals heterostructures and devices. *Nature Reviews Materials*, **1**(9):16042, (2016).
- [49] A M van der Zande, P Y Huang, D A Chenet, T C Berkelbach, Y You, G H Lee, T F Heinz, D R Reichman, D A Muller, and J C Hone. Exploring atomic defects in molybdenum disulphide monolayers. *Nature materials*, **12**:554–561, (2013).
- [50] Jeppe V. Lauritsen, Jakob Kibsgaard, Stig Helveg, Henrik Topsøe, Bjerne S. Clausen, Erik Lægsgaard, and Flemming Besenbacher. Size-dependent structure of MoS<sub>2</sub> nanocrystals. *Nature Nanotechnology*, **2**(1):53–58, (2007).
- [51] Xu Zhou, Jingxin Cheng, Yubing Zhou, Ting Cao, Hao Hong, Zhimin Liao, Shiwei Wu, Hailin Peng, Kaihui Liu, and Dapeng Yu. Strong second-harmonic generation in atomic layered GaSe. *Journal of the American Chemical Society*, **137**(25):7994–7997, (2015).
- [52] Kaihui Liu, Liming Zhang, Ting Cao, Chenhao Jin, Diana Qiu, Qin Zhou, Alex Zettl, Peidong Yang, Steve G. Louie, and Feng Wang. Evolution of interlayer coupling in twisted molybdenum disulfide bilayers. *Nature Communications*, **5**:4966, (2014).
- [53] Mei Yang, Xuerui Cheng, Yuanyuan Li, Yufen Ren, Miao Liu, and Zeming Qi. Anharmonicity of monolayer MoS<sub>2</sub>, MoSe<sub>2</sub>, and WSe<sub>2</sub>: A Raman study under high pressure and elevated temperature. *Applied Physics Letters*, **110**(9):093108, (2017).
- [54] Woosuk Choi, Imtisal Akhtar, Malik Abdul Rehman, Minwook Kim, Dongwoon Kang, Jongwan Jung, Yoon Myung, Jungcheol Kim, Hyeonsik Cheong, and Yongho Seo. Twist-angle-dependent optoelectronics in a few-layer transition-metal dichalcogenide heterostructure. *ACS Applied Materials & Interfaces*, **11**(2):2470–2478, (2019).
- [55] Lama Khalil, Debora Pierucci, Emilio Velez-Fort, José Avila, Céline Vergnaud, and Pavel Dudin. Hybridization and localized flat band in the WSe<sub>2</sub>/MoSe<sub>2</sub> heterobilayer. *Nanotechnology*, **34**:045702, (2023).

- [56] Xin Zhang, Xiao-Fen Qiao, Wei Shi, Jiang-Bin Wu, De-Sheng Jiang, and Ping-Heng Tan. Phonon and raman scattering of two-dimensional transition metal dichalcogenides from monolayer, multi-layer to bulk material. *Chem. Soc. Rev.*, **44**:2757–2785, (2015).
- [57] Biswanath Chakraborty, Achintya Bera, D. V. S. Muthu, Somnath Bhowmick, U. V. Waghmare, and A. K. Sood. Symmetry-dependent phonon renormalization in monolayer MoS<sub>2</sub> transistor. *Phys. Rev. B*, **85**:161403, (2012).
- [58] Changgu Lee, Hugen Yan, Louis E. Brus, Tony F. Heinz, James Hone, and Sunmin Ryu. Anomalous lattice vibrations of single and few-layer MoS<sub>2</sub>. *ACS Nano*, **4**(5):2695–2700, (2010).
- [59] A. Molina-Sánchez and L. Wirtz. Phonons in single-layer and few-layer MoS<sub>2</sub> and WS<sub>2</sub>. *Phys. Rev. B*, **84**:155413, (2011).
- [60] Xin Lu, M. Iqbal Bakti Utama, Junhao Lin, Xue Gong, Jun Zhang, Yanyuan Zhao, Sokrates T. Pantelides, Jingxian Wang, Zhili Dong, Zheng Liu, Wu Zhou, and Qihua Xiong. Large-area synthesis of monolayer and few-layer MoSe<sub>2</sub> films on SiO<sub>2</sub> substrates. *Nano Letters*, **14**(5):2419–2425, (2014).
- [61] Jing-Kai Huang, Jiang Pu, Chang-Lung Hsu, Ming-Hui Chiu, Zhen-Yu Juang, Yung-Huang Chang, Wen-Hao Chang, Yoshihiro Iwasa, Taishi Takenobu, and Lain-Jong Li. Large-area synthesis of highly crystalline WSe<sub>2</sub> monolayers and device applications. *ACS Nano*, **8**(1):923–930, (2014).
- [62] J. Binder, J. Howarth, F. Withers, M. R. Molas, T. Taniguchi, K. Watanabe, C. Faugeras, A. Wysmolek, M. Danovich, V. I. Fal’ko, A. K. Geim, K. S. Novoselov, M. Potemski, and A. Kozikov. Upconverted electroluminescence via Auger scattering of interlayer excitons in van der Waals heterostructures. *Nature Communications*, **10**(1):2335, (2019).
- [63] Cheng-Syuan Cai, Wei-Yan Lai, Po-Hsuan Liu, Tzu-Chieh Chou, Ro-Ya Liu, Chih-Ming Lin, Shangjr Gwo, and Wei-Ting Hsu. Ultralow Auger-assisted interlayer exciton annihilation in WS<sub>2</sub>/WSe<sub>2</sub> Moiré heterobilayers. *Nano Letters*, **24**(9):2773–2781, (2024).